Fast Detection and Segmentation of Drusen in Retinal Optical Coherence Tomography Images

Sina Farsiu[a#], Stephanie J. Chiu[b], Joseph A. Izatt[b,a], Cynthia A. Toth[a,b]

[a]Department of Ophthalmology, Duke University Medical Center, Durham, NC, 27710, USA
[b]Department of Biomedical Engineering, Duke University, Durham, NC, 27710, USA

ABSTRACT

Accurate detection-characterization of drusen is an important imaging biomarker of age-related macular degeneration (AMD) progression. We report on the development of an automatic method for detection and segmentation of drusen in retinal images captured via high speed spectral domain optical coherence tomography (SDOCT) systems. The proposed algorithm takes advantage of *a priori* knowledge about the retina shape and structure in the AMD and normal eyes. In the first step, the location of the retinal nerve fiber layer (RNFL) is estimated by searching for the locally connected segments with high radiometric vertical gradients appearing in the upper section of the SDOCT scans. The high reflective and locally connected pixels that are spatially located below the RNFL layer are taken as the initial estimate of the retinal pigment epithelium (RPE) layer location. Such rough estimates are smoothed and improved by using a slightly modified implementation of the Xu-Prince gradient vector flow based deformable snake method. Further steps, including a two-pass scan of the image, remove outliers and improve the accuracy of the estimates. Unlike healthy eyes commonly exhibiting a convex RPE shape, the shape of the RPE layer in AMD eyes might include abnormalities due to the presence of drusen. Therefore, by enforcing local convexity condition and fitting second or fourth order polynomials to the possibly unhealthy (abnormal) RPE curve, the healthy (normal) shape of the RPE layer is estimated. The area between the estimated normal and the segmented RPE outlines is marked as possible drusen location. Moreover, fine-tuning steps are incorporated to improve the accuracy of the proposed technique. All methods are implemented in a graphical user interface (GUI) software package based on MATLAB platform. Minor errors in estimating drusen volume can be easily manually corrected using the user-friendly software interface and the program is constantly refined to correct for the repeating errors. This semi-supervised approach significantly reduces the time and resources needed to conduct a large-scale AMD study. The computational complexity of the core automated segmentation technique is attractive as it only takes about 6.5 seconds on a conventional PC to segment, display, and record drusen locations in an image of size (512 × 1000) pixels. Experimental results on segmenting drusen in SDOCT images of different subjects are included, which attest to the effectiveness of the proposed technique.

Keywords: Spectral Domain Optical Coherence Tomography, Segmentation, Drusen, Age-Related Macular Degeneration, Retinal Pigment Epithelium, Ophthalmic Imaging, Retina, Duke OCT Retinal Analysis Program, DOCTRAP

1. INTRODUCTION

Age-related macular degeneration is the leading cause of severe visual impairment in patients over the age of 65 in the developed world.[1] An estimated 8 million persons at least 55 years old in the United States have monocular or binocular intermediate AMD or monocular advanced AMD.[2] Drusen* are accumulations of extracellular material (proteins and lipids) between the RPE and inner collagenous layer of Bruch's membrane of the eye. Early, fast, and accurate detection of drusen is of great importance to the ophthalmology community since the size of drusen is considered as an early indicator of AMD progression.[3,4]

#Corresponding Author:
E-mail: sina.farsiu@duke.edu, Telephone: (1)919-684-6642, Webpage: http://www.duke.edu/~sf59/

*Note that in this report, to improve readability, regardless of size, we refer to all such deposits as drusen. E.g. rather than calling a deposit with diameter larger than 300-500 μm "drusenoid pigment epithelial detachment", we simply refer to it as druse.

Ophthalmic Technologies XVIII, edited by Fabrice Manns, Per G. Söderberg, Arthur Ho, Bruce E. Stuck, Michael Belkin, Proc. of SPIE Vol. 6844, 68440D, (2008) · 1605-7422/08/$18 · doi: 10.1117/12.768624

For decades, the gold standard for *in vivo* drusen imaging has been color fundus photography. In epidemiologic studies, observers evaluate color fundus photographs of drusen for morphologic features such as distinctness, individual size, number, and estimated total area of drusen. Such assessment of severity of disease is still used to predict AMD progression, even though agreement among observers is moderate.[5] This, among many other limitations of fundus photography, has motivated the ophthalmic practitioners to search for alternative retinal imaging systems.

High-resolution optical imaging of objects hidden in scattering media such as the human eye is a challenging and important problem with many industrial and medical applications. To achieve this goal and create virtually blur free images, several imaging systems have been developed that separate the ballistic photons which travel through the scattering medium in a straight line from the scattered ones.[6] Optical coherence tomography (OCT), first reported[7] in 1991, is such a system and has been rapidly adapted for medical applications, especially for ophthalmic imaging purposes.[8–11]

By employing an interferometer,[12,13] several OCT based imaging systems have been developed through out the years, most notably the time-domain OCT (TDOCT), ultrahigh resolution OCT[14] (UHROCT), and very recently SDOCT.[15,16] In the classic TDOCT systems only the photons from a preselected layer contribute in generating the interferometric signal. A widely used clinical TDOCT system commercially known as the Stratus-OCT (Carl Zeiss Meditec, Dublin, CA) acquires 512 axial scans (A-scans) of 8 to 10 micron axial resolution in about 1.28 seconds. A related more recent UHROCT technology, which employs femto-second (fs) lasers as the light source, on the other hand provides images with axial resolutions of 2 to 3 microns, demonstrating retinal morphology in much improved detail. Unfortunately, these systems are often slower than the TDOCT systems (approximately 150 to 250 axial scans per second)[17] and, moreover, utilization of the fs lasers in a commercial OCT system is complex and expensive.

Fortunately, development and utilization of the novel SDOCT systems has enabled us to acquire images many times faster than the classic TDOCT systems, with higher resolution and better signal-to-noise-ratio (SNR).[18] Unlike their critically slow time-domain predecessors, in SDOCT the interference signal is a function of optical wavelength, simultaneously measuring all echoes of light from different layers. This property enables the state-of-the-art SDOCT imaging systems to capture tens of high-resolution and high-SNR frames, with the axial-resolution of less than 5 microns, in less than one second. In fact, SDOCT imaging is 50 times faster than standard TDOCT and 100 times faster than UHROCT imaging systems.[17] Future SDOCT systems will go even further, acquiring 3-D scans with the speed of hundreds of high-resolution frames per second.

The improved imaging of drusen is one of the major evolutionary steps in AMD studies achieved with SDOCT. With SDOCT and UHROCT systems, entire drusen can be imaged, facilitating the *in vivo* critical analysis of substructural details.[14] It should be noted that tomographic and radiometric variability in drusen appearance can be only seen in the SDOCT and UHROCT images, while color fundus photography may suggest much more phenotypic homogeneity. In other words, while in a color fundus photograph several drusen may appear similar, SDOCT reveals significant differences in drusen substructure.[19]

As mentioned in the previous paragraphs, the novel SDOCT systems provide 3-D scans with the speed of tens to hundreds of high-resolution frames per second. In many practical cases, including large scale studies that involve imaging hundreds of subjects in a short period of time, the massive amount of information generated by the SDCOCT systems is often too large and time consuming to be fully analyzed and interpreted by human experts. Therefore, the need for the development of automatic or semi-automatic computer-vision based image/video analysis systems that expedite the decision making process of ophthalmic experts is now sensed more than ever.

The image processing based computer aided diagnosis algorithms for OCT images have recently been of great interest in AMD studies. For example, recently a semi-automatic technique for segmenting the fluid-filled regions associated with neovascular AMD in OCT images is developed.[20] In that work, as a prerequisite step for segmentation, a speckle noise reduction algorithm is proposed, which is mainly based on the edge adaptive anisotropic diffusion[21] methodology, and the semi-automatic segmentation step is based on the gradient vector flow snake[22] algorithm (which is also used in our algorithm).

As the abnormal thickness of different retinal layers is also an indicator of the AMD development, some efforts are focused on automatic (or at least semi-automatic) measurement of these layers. Unfortunately, software accompanying commercial OCT systems often do not have the accuracy needed for scientific studies, and such errors are reported in previous studies.[23,24] As an alternative, an ad-hoc approach specially modified to be used for images captured by the Stratus-OCT systems[25] is recently developed to discriminate normal from glaucomatous eyes. Another automated segmentation approach for the separation of the retina into five layers on 3-D macular OCT scans has been developed.[26] Very recently a related technique based on transforming the segmentation task into finding a minimum-cost closed set in a geometric graph constructed from local edge information and enforcing surface smoothness and interaction constraints is suggested for segmenting retina to five layers.[27,28]

While current methods of detecting drusen area in fundus photos are done either manually or automatically, most mentioned studies in the above paragraph are based on TDOCT systems, very few papers have addressed the problem of segmenting drusen in SDOCT images. To the best of our knowledge, most studies in this field are based on manual segmentation of drusen.[29] Very recently, while this paper was under final revision, a semi-automatic method of detecting drusen in SDOCT images is published.[30] This support vector machine based semi-automatic segmentation method requires some interaction with ophthalmic expert, including sparse manual markings of drusen locations. In the next section, we introduce a fast automatic technique for detecting subretinal pathology in the form of drusen in the SDOCT images.

2. METHODS

In this paper, drusen in each frame is independently detected and segmented, reducing the memory and computational requirements. As we note in Section 4, a simultaneous joint 3D segmentation technique, might provide better results, with increased memory requirement and computational complexity. The core drusen segmentation algorithm is implemented in several steps, including many minor details. The outline of this algorithm is described in this section.

While for the purpose of drusen segmentation, accurate segmentation of the RNFL layer is not necessary, a rough estimate of this layer can effectively reduce drusen segmentation outliers. This is especially important for the cases of abnormal retinal scans, where the RNFL layer is significantly brighter than the RPE layer. Compared to the RPE, detection of the RNFL layer is a relatively simple task, as the area above the RNFL layer often appears as uniform low-reflectivity background noise, creating a vivid structural contrast. In the first step, the image SNR is improved by low-pass filtering the raw scans, reducing the speckle noise. A simple high-pass filtering of this denoised image (e.g. by convolving the image with a vertical edge kernel) highlights the outline of the RNFL layer as sparsely connected high-intensity pixels in the upper section of the image. Later, this image is blurred in the horizontal direction, further reducing the disconnected (possibly false) edges. By comparing the noise power in the background to this edge image, most background pixels are detected and marked to be left out of the RNFL search space. Simple morphological operators[†] are then used to remove high intensity disconnected outlier pixels. Finally, by enforcing smoothness condition, the sparsely detected pixels are locally connected, creating an outline of the RNFL layer.

In the next step, the area below the estimated RNFL layer is searched for the RPE layer. In this case, with high probability, at least a few RPE pixels attain the highest pixel values in the search area. In a noise filtered image, first, the highest locally connected pixels are marked. Starting from the left side of the image, the brightest pixels in the local approximates of the already detected RPE estimates are detected. The output of this step is a rough estimate of the RPE layer. A more smooth, yet locally loyal to the edge structure, RPE shape is later generated by using this rough estimate as an initial guess for the gradient vector flow based deformable snake method.[22] Starting from the right side of the image, this process is repeated, creating a possibly different estimate of the RPE (due to different initialization point). By fusing these two estimates of the RPE layer, a more reliable RPE approximation is created. Since hyper-reflective debris are sometime attached to the RPE (as overlying bright spots), if no other discriminating factor is detected between these two estimates, the locally lower positioned estimate is incorporated to define the final RPE estimate.

[†]e.g. *bwareaopen* function in MATLAB.

After detecting the RPE layer location, its shape is analyzed for distortions in the form of local bumps or elevations, representing possible drusen locations. By enforcing convexity condition and locally fitting a second or fourth order polynomial to this possibly unhealthy (abnormal) RPE curve, the healthy (normal) shape of the RPE layer is estimated. The area between the estimated normal and the segmented RPE outlines is marked as possible drusen location. Moreover, fine-tuning steps are incorporated to improve the accuracy of the proposed technique.

All image processing methods and graphical user-interfaces are implemented in a software package called "Duke OCT Retinal Analysis Program" (DOCTRAP), which is currently based on MATLAB R.2007.b (Mathworks, Natick, MA) environment. Since drusen appearance in locations closer to the fovea is of greater diagnosis and prognosis importance, the user has been given the choice of selecting an arbitrary region of interest (ROI) (e.g. a 3.6 mm diameter circle centered around the fovea as in Figure 1) [‡]. To facilitate the ROI selection task, by collapsing captured images (summation of all pixels) on an axial line, a two-dimensional image analogous to a fundus image, called the summed voxel projection (SVP),[24,31] is created. Drusen segmentation is performed only in the ROI section, further speeding up the process. More importantly, quantitative measurements (e.g. total drusen volume) which are automatically reported by the software, only reflect the analytic results in the ROI section.

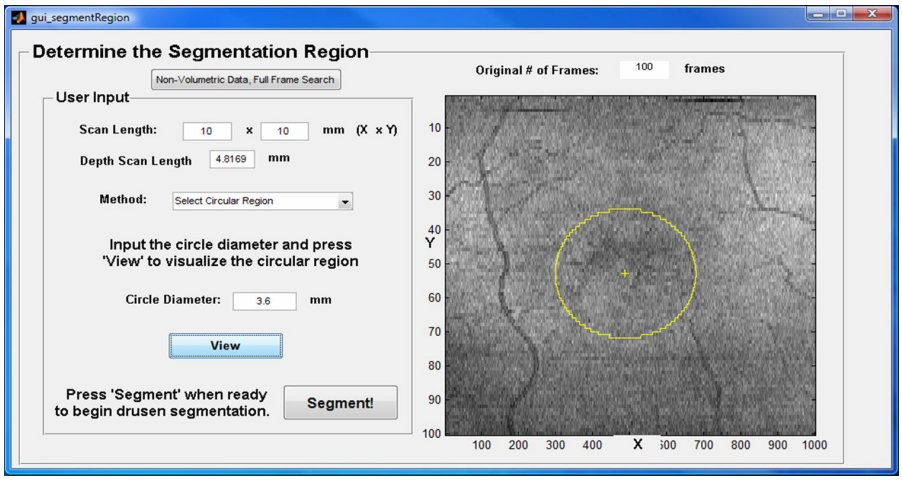

Figure 1. Screenshot of the software's ROI selection page. The SVP image (shown on the right side) is automatically generated and the user has the choice of defining an arbitrary shaped or a circular ROI around the fovea (the yellow circle). The user may also reflect SDOCT scan properties used for imaging, e.g. the scan depth and length, to generate customized quantitative analysis and measurements reports. Note that fovea location is selected using a separate full frame browsing GUI.

The automatic segmentation step is relatively fast (a full frame analysis including segmentation, display, and saving results takes about 6.5 seconds on an Intel Centrino-Duo 2.4 GHz CPU) and it can be executed off-line. The results of the automated segmentation step are displayed in a user-friendly GUI, to be examined or possibly modified by ophthalmic experts. A screenshot of the software's display/modification GUI is shown in Figure 2. Drusen area and outline, ROI, RPE, RNFL, relative location of the frame on SVP, and other useful features are marked on different parts of this GUI. Note that, while the rough initial segmentation is done in full frame, the enhancement steps are only done in the ROI. Aside from the automatically generated drusen characterization reports (number of drusen, volume, etc.), the user may also take advantage of the manual measurement tools.

[‡]Alternatively, the program may automatically analyze the whole scan set, without any user interaction.

The user may chose the Freehand or other editing tools to modify the automated segmentation results. The segmented images can be saved in various formats, including, MATLAB "mat" files, EPS, TIF, and PNG. The quantitative results are exported in "mat", text, and even Microsoft Excel formats.

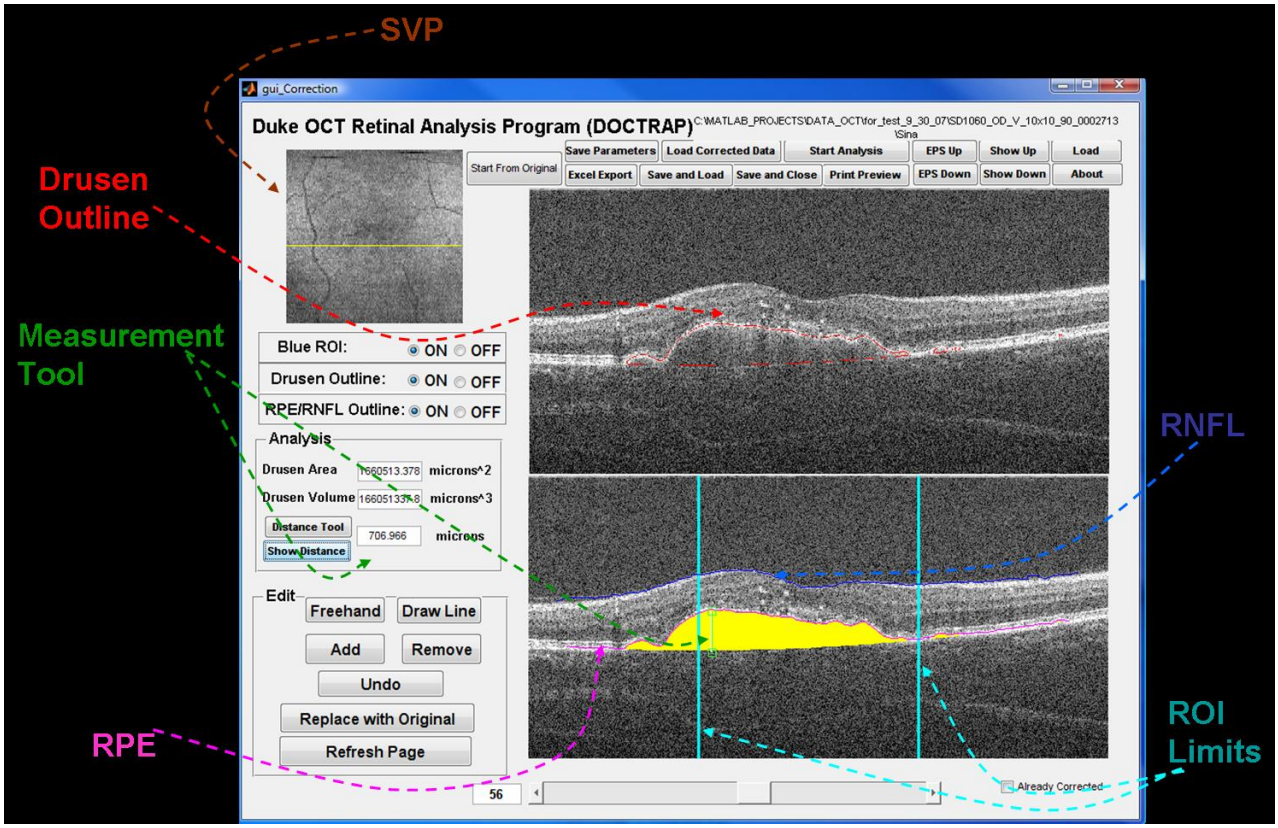

Figure 2. A screenshot of the software's main GUI, where the user may visualize and modify the outcome of the automatic segmentation algorithm. The outline of detected drusen is overlayed on the raw SDOCT scan and marked by the red dashed-line in the top-right image. The drusen area is colored in yellow in the down-right image. The corresponding location of the scan on the SVP is marked with a yellow line on the left-top section of the GUI. A blue and a red line, mark the RNFL and RPE locations on the down-right image, respectively. As a point of reference, the vertical blue lines in the down-right image show the ROI boundaries originally selected in the GUI of Figure 1. Note that, while the initial segmentation is done in full frame, the accurate final segmentation is only done in the ROI.

3. RESULTS

A clinical SDOCT system was used to acquire images of eyes with Age-Related Eye Disease Study Level 3 AMD. Study consent was obtained from all subjects and the study protocol was approved by the Duke University Medical Center institutional review board. The system (Bioptigen, Inc. Durham, NC) uses a low-coherence laser diode centered at 840 nm with a bandwidth of 49 nm. Using software from Bioptigen, Inc., sets of 100 volumetric scan frames of size 512 (axial) $\times$ 1000 (lateral) are acquired in 6.7 seconds.

Using the methods and software explain in the previous section, we examined six AMD eyes, each with a $3.6mm$ ROI centered at the fovea, effectively segmenting a total of 228 SDOCT B-scans. These images were also segmented manually by two ophthalmic experts. A selected number of frames representing common patterns seen in the segmented images are reported in this section.

Figure 3, shows an example of detecting a large druse, pigment epithelial detachments (PED), in an SDOCT scan. Figure 3.a, shows the display screenshot viewed by the user (including the rough initial estimates of the

RPE, RNFL, and drusen outside the ROI). Figures 3.b-c, show the magnified raw and drusen segmented (yellow region inside the blue ROI lines) images, respectively. Note that, our double scan method, has correctly ignored the hyper-reflective debris, marked by the "A" and "B" red arrows, overlaying the true drusen area. This is an important feature of our algorithm, reducing the time needed to manually correct for the mistakenly segmented regions.

Figure 4, shows an example of detecting drusen of different shapes and sizes in a single scan. The abnormal hyper-reflective epiretinal membrane (appearing brighter than RPE) and the hyper-reflective debris overlaying the central druse, did not affect the performance of the robust segmentation algorithm.

Figure 5 shows an example of detecting drusen of different shape and size in a single scan. The abnormal hyper-reflective epiretinal membrane (brighter than RPE) did not affect the performance of the robust segmentation algorithm and all medium sized drusen inside the ROI were correctly segmented as shown in Figure 5.b.

Figure 6 shows an example of detecting three small sized distinct drusen. As shown in Figure 6.b, all small sized drusen inside the ROI were correctly segmented.

Figure 7.a shows an example of a scan with a single very small sized druse inside ROI. Figure 7.b shows that even this very small sized druse is correctly detected and segmented.

Figure 8.a shows an example of a scan with a single small abnormally shaped druse, marked by the red arrow "A", and one extremely small sized normal druse, marked by the red arrow "B". Note that, at location "A", the shape of the RPE is not changed and therefore the algorithm has missed detecting this drusen. Yet, the smaller sized "normal" druse at location "B", where the RPE shape is deformed, is correctly detected. We hypothesize that the undetected druse might have different origin and medical significance, compared to common drusen seen in SDOCT scans of AMD eyes. We will report on detecting this type of drusen and their medical implications in our future publications.

Figure 9.a shows an example of a scan with a single large druse, with two types of automatic segmentation errors. Accumulation of hyper-reflective debris over PED, has resulted in the small erroneously segmented bulge marked by the red arrow "A" in Figure 9.b. However, the effect of the hyper-reflective subretinal debris was remarkably nullified in the area marked by the red arrow "B", resulting in correct segmentation. The red arrow "C" marks the second type of error associated with our algorithm, where the lower boundary of the segmented druse is slightly higher than the faint line supposedly marking the drusen border. Enhancing the algorithm to correct for these errors is part of our ongoing work.

4. DISCUSSION AND FUTURE WORK

The developed software based on our proposed algorithm accurately segments drusen in the SDOCT images of AMD eyes. Inevitable errors can be manually corrected using the user-friendly software interface and the program is constantly refined to correct for the repeating errors. This semi-supervised approach significantly reduces the time and resources needed to conduct a large-scale AMD study.

Some automatic segmentation errors, such as missing the abnormal drusen of Figure 8, might indicate different classes of drusen each with specific medical implications. Also, some false regions may be mistakenly marked as drusen in eyes with RPE elevation unrelated to drusen. We will report on this in our future publications. We also note that since our technique segments drusen in single (independent) slices, regardless of the neighboring scans, its performance might be suboptimal. Fortunately, it is possible to modify our system to perform simultaneous segmentation of 3D volumetric scans with superior performance (and inevitable increased memory requirements and CPU computation time). We will report on the performance of such 3D segmentation system in our upcoming publications.

Automatic categorization of drusen ultrastructure in SDOCT scans of AMD eyes is part of our ongoing work. Manual morphologic categorization of drusen based on ad-hoc definitions of shape, predominant internal reflectivity, homogeneity, and presence of overlying hyper-reflective foci is previously reported. An automated system, with mathematically defined drusen characteristics, will result in more accurate, reliable, and repeatable categorization of drusen. We will report on this in an upcoming publication.[32]

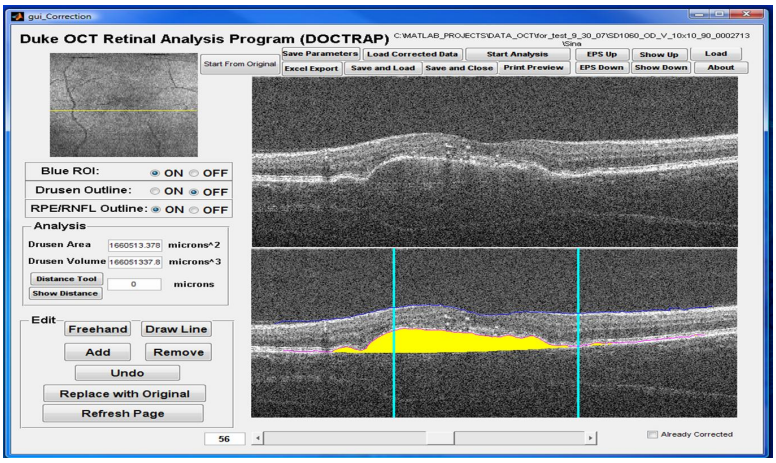

a

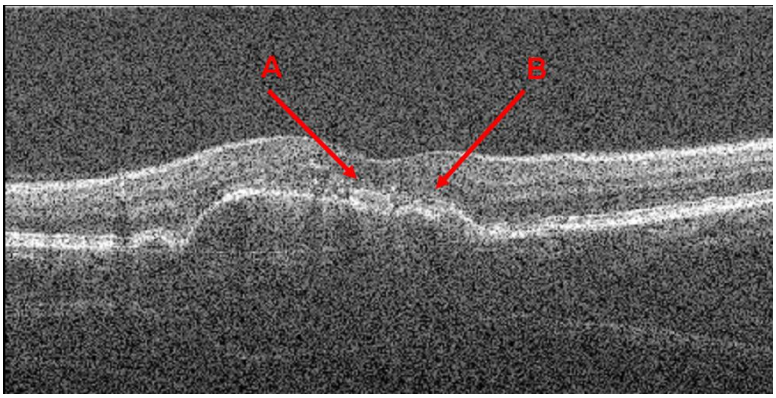

b

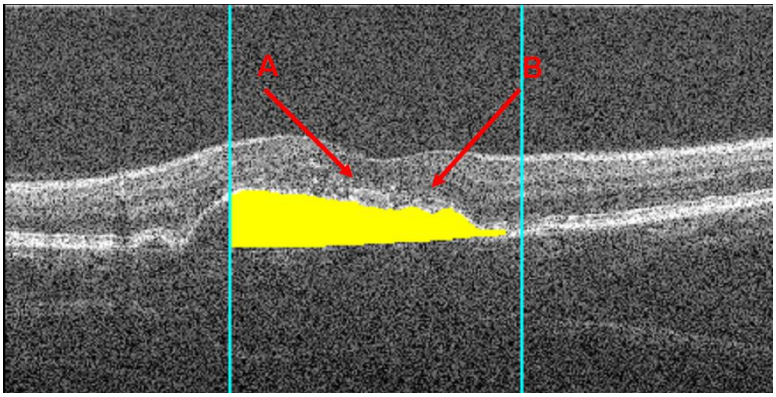

c

Figure 3. (a) Screenshot of the software's main GUI, and markings of the drusen on the whole frame. Note that only drusen located between the blue lines are accurately segmented and reported. (b)-(c) The user can magnify the original raw and marked images, displaying drusen area located inside the ROI. Due to the large size, detection of drusen in this image is a fairly easy task. However, our algorithm is able to correctly ignore the hyper-reflective debris overlaying the PED (marked by the red A and B arrows) and report accurate volume.

Finally, while our method shows robustness with respect to the measurement and speckle noise in SDOCT images, it is natural to expect more accurate segmentation results in less-noisy higher-resolution images. We will report on this, and other aspects of our research in our upcoming publications.[24,33]

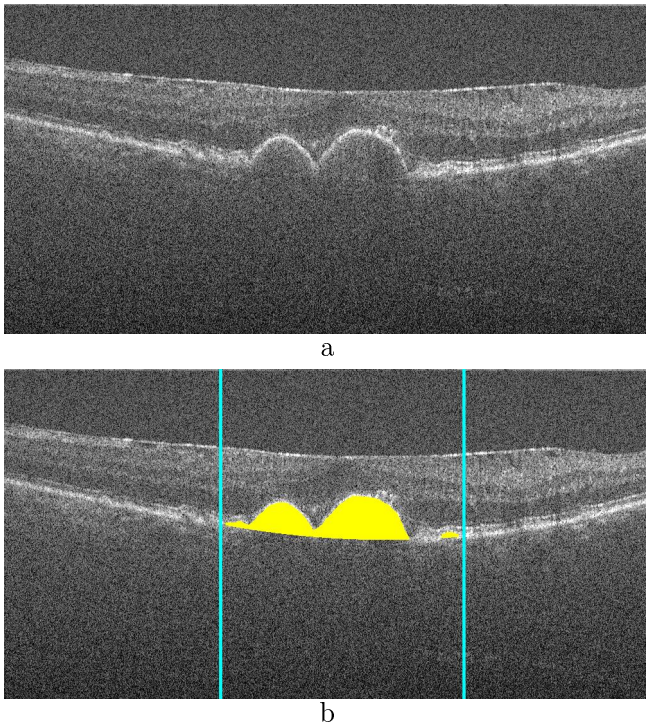

a

b

Figure 4. (a) A raw SDOCT scan of an AMD eye, with abnormally hyper-reflective epiretinal membrane (appearing brighter than RPE) and hyper-reflective debris overlaying the central druse. (b) The processed image showing the automatically segmented drusen (of different size and shape) in yellow, located inside the blue line marking the ROI.

ACKNOWLEDGMENTS

Authors wish to thank Dr. Neeru Sarin, Katrina Winter, Michelle McCall, Dr. Aziz A. Khanifar, Bradley A. Bower, and Amy Motomura for providing invaluable insight throughout this project. This work was supported in part by National Institutes of Health grant R21EY017393, National Institutes of Health Small Business Investigational Grant Subcontract from Bioptigen Inc., and by North Carolina Biotechnology Center Collaborative Funding Grant ♯2007-CFG-8005, entitled, "Improving Imaging of Phenotypes in Age-Related Macular Degeneration".

REFERENCES

1. R. Klein, B. Klein, S. Jensen, and S. Meuer, "The five-year incidence and progression of age-related maculopathy: the Beaver Dam Eye Study.," *Ophthalmology* **104**(1), pp. 7–21, 1997.
2. S. In, "Photodynamic Therapy of Subfoveal Choroidal Neovascularization With Verteporfin Fluorescein Angiographic Guidelines for Evaluation and Treatment-TAP and VIP Report No. 2," 2003.
3. D. Pauleikhoff, M. Barondes, D. Minassian, I. Chisholm, and A. Bird, "Drusen as risk factors in age-related macular disease.," *American Journal of Ophthalmology* **109**(1), pp. 38–43, 1990.
4. G. Hageman, P. Luthert, N. Victor Chong, L. Johnson, D. Anderson, and R. Mullins, "An Integrated Hypothesis That Considers Drusen as Biomarkers of Immune-Mediated Processes at the RPE-Bruch's Membrane Interface in Aging and Age-Related Macular Degeneration," *Progress in Retinal and Eye Research* **20**(6), pp. 705–732, 2001.
5. Age-related eye disease study research group (AREDS), "The age-related eye disease study system for classifying age-related macular degeneration from stereoscopic color fundus photographs: the age-related eye disease study report number 6. ," *Am. J. Ophthalmol.* **132**, pp. 668–681, 2001.

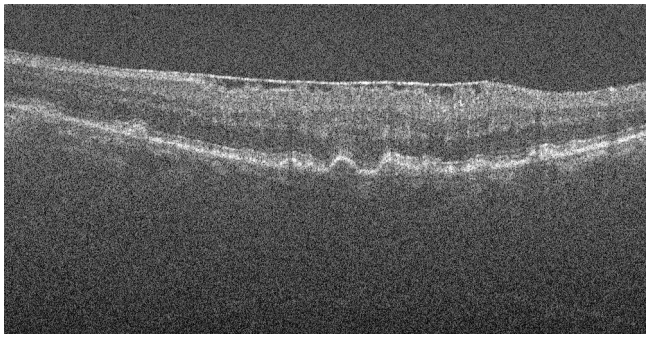

a

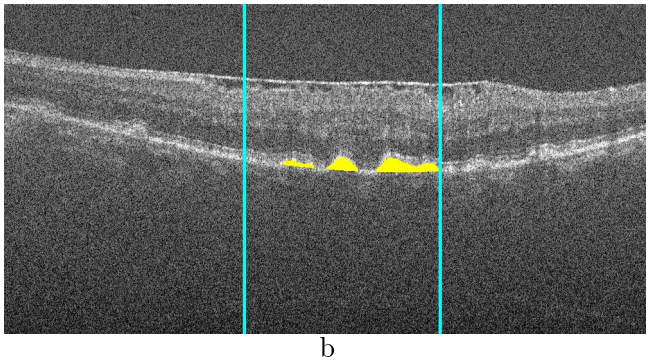

b

Figure 5. (a) A raw SDOCT scan of an AMD eye, with abnormally hyper-reflective epiretinal membrane (brighter than RPE) and medium size drusen. (b) The processed image showing the automatically segmented drusen (of different size and shape) in yellow, inside the blue ROI line.

6. S. Farsiu, J. Christofferson, B. Eriksson, P. Milanfar, B. Friedlander, A. Shakouri, and R. Nowak, "Statistical Detection and Imaging of Objects Hidden in Turbid Media Using Ballistic Photons," *Applied Optics* **47**(22), pp. 5805–5822, 2007.
7. D. Huang, E. Swanson, C. Lin, J. Schuman, W. Stinson, W. Chang, M. Hee, T. Flotte, K. Gregory, C. Puliafito, *et al.*, "Optical coherence tomography," *Science* **254**(5035), pp. 1178–1181, 1991.
8. M. Hee, J. Izatt, E. Swanson, D. Huang, J. Schuman, C. Lin, C. Puliafito, and J. Fujimoto, "Optical coherence tomography of the human retina," *Archives of Ophthalmology* **113**(3), pp. 325–332, 1995.
9. C. Toth, R. Birngruber, S. Boppart, M. Hee, J. Fujimoto, C. DiCarlo, E. Swanson, C. Cain, D. Narayan, G. Noojin, *et al.*, "Argon laser retinal lesions evaluated in vivo by optical coherence tomography.," *Am J Ophthalmol* **123**(2), pp. 188–98, 1997.
10. D. Hess, S. Asrani, M. Bhide, L. Enyedi, S. Stinnett, and S. Freedman, "Macular and retinal nerve fiber layer analysis of normal and glaucomatous eyes in children using optical coherence tomography," *American Journal of Ophthalmology* **139**(3), pp. 509–517, 2005.
11. V. Srinivasan, M. Wojtkowski, A. Witkin, J. Duker, T. Ko, M. Carvalho, J. Schuman, A. Kowalczyk, and J. Fujimoto, "High-Definition and 3-dimensional Imaging of Macular Pathologies with High-speed Ultrahigh-Resolution Optical Coherence Tomography," *Ophthalmology* **113**(11), pp. 2054–2054, 2006.
12. A. F. Fercher, W. Drexler, C. K. Hitzenberger, and T. Lasser, "Optical coherence tomography - principles and applications," *Reports on Progress in Physics* **66**(2), pp. 239–303, 2003.
13. C. Dunsby and P. M. W. French, "Techniques for depth-resolved imaging through turbid media including coherence-gated imaging," *J. Phys. D: Appl. Phys.* **36**, pp. 207–227, July 2003.
14. C. Pieroni, A. Witkin, T. Ko, J. Fujimoto, A. Chan, J. Schuman, H. Ishikawa, E. Reichel, and J. Duker, "Ultrahigh resolution optical coherence tomography in non-exudative age related macular degeneration," *British Medical Journal* **90**(2), pp. 191–197, 2006.

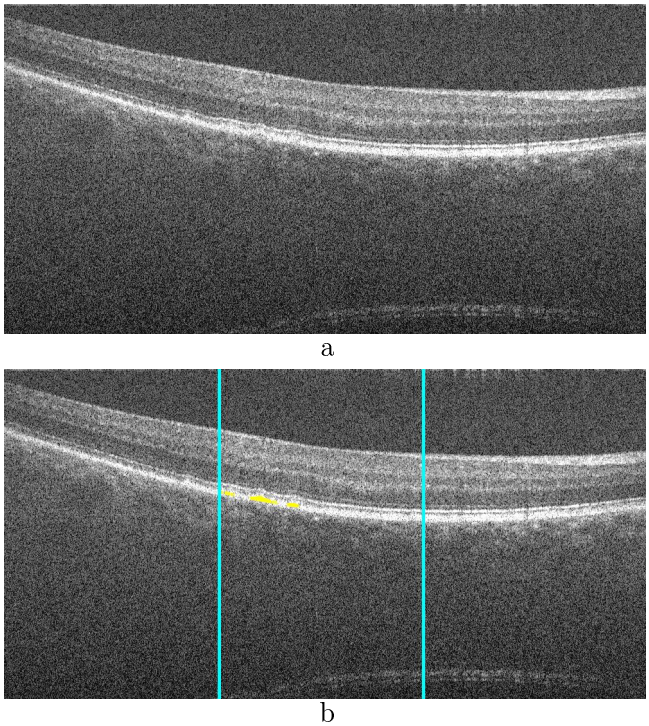

a b

Figure 6. (a) A raw SDOCT scan of an AMD eye, with three small sized distinct drusen. (b) The processed image shows the automatically segmented drusen (inside the blue ROI line) in yellow.

15. M. Choma, M. Sarunic, C. Yang, and J. A. Izatt, "Sensitivity advantage of swept source and Fourier domain optical coherence tomography," *Optics Express* **11**(18), pp. 2183–2189, 2003.
16. N. Iftimia, D. Hammer, C. Bigelow, T. Ustun, A. Burbo, J. de Boer, and R. Ferguson, "Hybrid LSLO/SDOCT retinal imager," *Ophthalmic Technologies XVII. Edited by Manns, Fabrice; Soederberg, Per G.; Ho, Arthur; Stuck, Bruce E.; Belkin, Michael. Proceedings of the SPIE,* **6426**, p. 642602, 2007.
17. M. Wojtkowski, V. Srinivasan, J. Fujimoto, T. Ko, J. Schuman, A. Kowalczyk, and J. Duker, "Three-dimensional Retinal Imaging with High-Speed Ultrahigh-Resolution Optical Coherence Tomography," *Ophthalmology* **112**(10), pp. 1734–1746, 2005.
18. J. de Boer, B. Cense, B. Park, M. Pierce, G. Tearney, and B. Bouma, "Improved signal-to-noise ratio in spectral-domain compared with time-domain optical coherence tomography," *Optics Letters* **28**(21), pp. 2067–2069, 2003.
19. A. A. Khanifar, A. F. Koreishi, J. A. Izatt, and C. A. Toth, "Drusen ultrastructure imaging with spectral domain optical coherence tomography in age-related macular degeneration," *Retina Society Meeting* , Oct. 2007.
20. D. Cabrera Fernández, "Delineating Fluid-Filled Region Boundaries in Optical Coherence Tomography Images of the Retina," *Medical Imaging, IEEE Transactions on* **24**(8), pp. 929–945, 2005.
21. P. Perona and J. Malik, "Scale-space and edge detection using anisotropic diffusion," *IEEE Transactions on Pattern Analysis and Machine Intelligence* **12**(7), pp. 629–639, 1990.
22. C. Xu and J. Prince, "Generalized gradient vector flow external forces for active contours," *Signal Processing* **71**(2), pp. 131–139, 1998.
23. S. Sadda, Z. Wu, A. Walsh, L. Richine, J. Dougall, R. Cortez, and L. LaBree, "Errors in Retinal Thickness Measurements Obtained by Optical Coherence Tomography," *Ophthalmology* **113**(2), pp. 285–293, 2006.
24. C. A. Toth, S. Farsiu, A. A. Khanifar, and G. T. Chong, "Application of spectral domain optical coherence tomography in age-related macular degeneration analysis," in *OCT in AMD*, G. Coscas, ed., Book chapter to be published 2008.

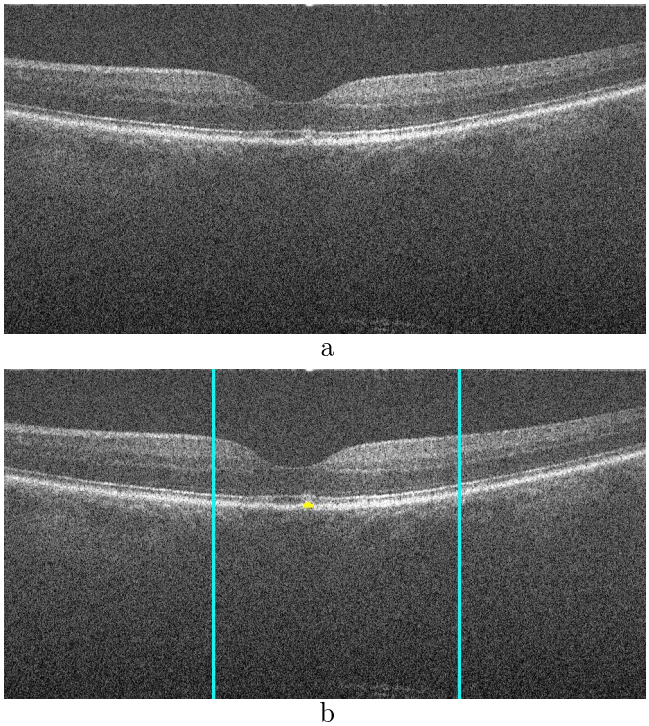

Figure 7. (a) A raw SDOCT scan of an AMD eye, with a single very small druse inside the ROI. (b) The processed image showing the automatically segmented druse (located inside the blue ROI line) in yellow.

25. H. Ishikawa, D. Stein, G. Wollstein, S. Beaton, J. Fujimoto, and J. Schuman, "Macular segmentation with optical coherence tomography," *Invest. Ophthalmol. Vis. Sci* **46**(6), pp. 2012–2017, 2005.
26. D. Cabrera Fernández, H. Salinas, and C. Puliafito, "Automated detection of retinal layer structures on optical coherence tomography images," *Optics Express* **13**(25), pp. 10200–10216, 2005.
27. M. Haeker, M. Abramoff, R. Kardon, and M. Sonka, "Segmentation of the Surfaces of the Retinal Layer from OCT Images," *LECTURE NOTES IN COMPUTER SCIENCE* **4190**, pp. 800–807, 2006.
28. M. Haeker, M. Sonka, R. Kardon, V. Shah, X. Wu, and M. Abràmoff, "Automated segmentation of intraretinal layers from macular optical coherence tomography images," *Proceedings of SPIE* **6512**, p. 651214, 2007.
29. B. Bower, S. Chiu, E. Davies, A. Davis, R. Zawadzki, A. Fuller, D. Wiley, J. Izatt, and C. Toth, "Development of quantitative diagnostic observables for age-related macular degeneration using Spectral Domain OCT," *Proceedings of SPIE* **6426**, p. 64260W, 2007.
30. A. Fuller, R. Zawadzki, S. Choi, D. Wiley, J. Werner, and B. Hamann, "Segmentation of Three-dimensional Retinal Image Data," *IEEE Transactions on Visualization and Computer Graphics* **13**(6), pp. 1719–1726, 2007.
31. S. Jiao, R. Knighton, X. Huang, G. Gregori, and C. Puliafito, "Simultaneous acquisition of sectional and fundus ophthalmic images with spectral-domain optical coherence tomography," *Optics Express* **13**(2), pp. 444–452, 2005.
32. C. A. Toth, S. Farsiu, S. J. Chiu, A. A. Khanifar, and J. A. Izatt, "Automatic drusen segmentation and characterization in spectral domain optical coherence tomography (sdoct) images of amd eyes," *Submitted to the 2008 the Association for Research in Vision and Ophthalmology (ARVO) Annual Meeting* , Apr. 2008.
33. S. Farsiu, B. A. Bower, J. A. Izatt, and C. A. Toth, "Image fusion based resolution enhancement of retinal spectral domain optical coherence tomography images," *Submitted to the 2008 the Association for Research in Vision and Ophthalmology (ARVO) Annual Meeting* , Apr. 2008.

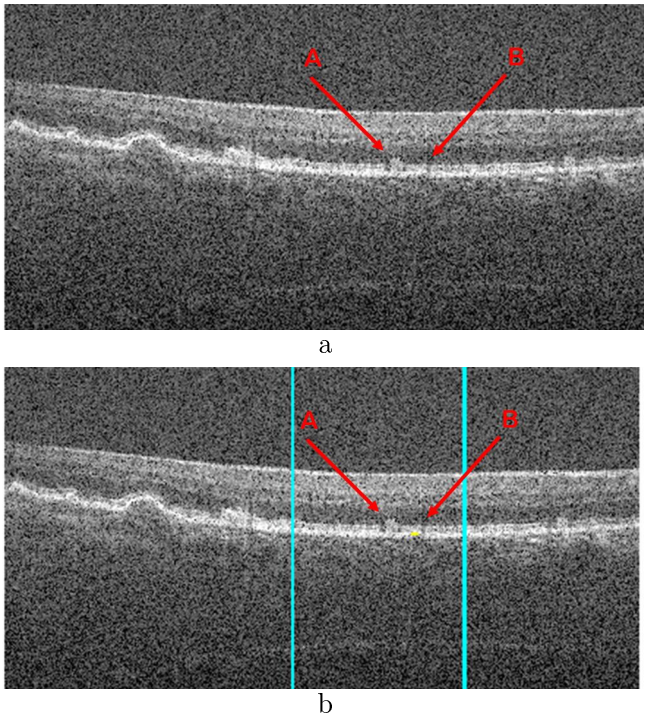

a

b

Figure 8. An example of the algorithm failing to detect abnormal drusen. (a) A raw SDOCT scan of an AMD eye, with a single small abnormally shaped druse marked by the red arrow "A", and one extremely small sized normal druse marked by the red arrow "B". Note that druse "A" has not changed the shape of the RPE. (b) The processed image showing the automatically segmented normal druse "B" in yellow. The abnormal druse "A" is missed, detection of which will be addressed in our future work.

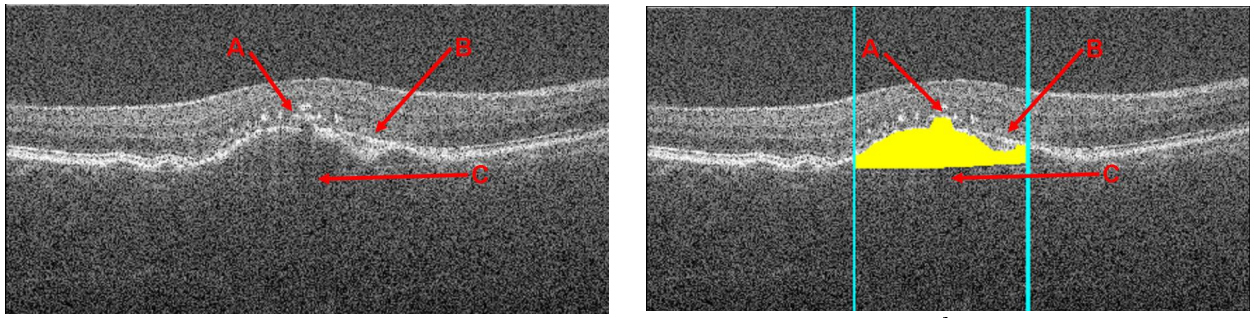

a b

Figure 9. An example of the algorithm failing to accurately mark drusen area. (a) A raw SDOCT scan of an AMD eye, with heavy accumulation of hyper-reflective debris over PED marked by the red arrow "A". Arrow "B" points to hyper-reflective outer retina elevated over a "valley" between two drusen. The red arrow "C", notes the faint line assumed to be the lower boundary of the druse. (b) The processed image showing the automatically segmented druse. The nipple shaped bulge marked with the red arrow "A" is mistakenly segmented as a part of the druse. The subretinal debris at site "B" are correctly left out of the druse area. The segmented druse does not touch the line marked with the red arrow "C", resulting in a lower estimate of the druse area. We will address this issues in our future work.